A Superresolution Wide Null Beamformer for Undersampled Signal Reconstruction in SIMO SAR

Karen Mak, *Student Member, IEEE*, and Athanassios Manikas, *Senior Member, IEEE*

***Abstract*—With single-input single-output (SISO) SAR systems, employing a single transmitter and receiver beam, there exists a high resolution, wide swath contradiction. However, by using multiple receiver beams and employing array processing techniques, this contradiction can be overcome, allowing greater flexibility and a wider range of application requirements to be met. In this paper the use of single-input multiple-output (SIMO) SAR systems for overcoming this contradiction is of interest, and a novel beamformer is proposed for processing in the cross-range direction. In order to fully describe the system, the array manifold vector is utilized, which is a key concept in the design of the beamformer. In particular, this beamformer is a superresolution beamformer capable of forming wide nulls using subspace based approaches and allows the suppression of ambiguities in multiple sets of received undersampled SAR data in the cross-range direction and reconstruction of the Doppler spectrum to form a single unambiguous set of SAR data. Compared to the existing reconstruction algorithm, only a single weighting vector is required for a block of ambiguous Doppler frequencies compared to a weight vector required for each ambiguous Doppler frequency. The capabilities of the proposed beamformer are shown to give an improved performance in ambiguity suppression via computer simulation studies in a representative maritime environment.**

***Index Terms*—Single-input multiple-output (SIMO) synthetic aperture radar (SAR), array manifold vector, array processing.**

NOTATION

a, A	Scalar
$\underline{a}, \underline{A}$	Column vector
$\mathbf{a}, \mathbb{A}$	Matrix
$\mathbb{I}_N$	$(N \times N)$ identity matrix
$\underline{1}_N$	$(N \times 1)$ vector of ones
$\underline{0}_N$	$(N \times 1)$ vector of zeros
$(\cdot)^T, (\cdot)^H$	Transpose, conjugate transpose
$diag\{\underline{a}\}$	Diagonal matrix whose diagonal entries the elements of $\underline{a}$
$\otimes$	Kronecker product
$\odot$	Hadamard (element-by-element) product

Manuscript received January 29, 2015; revised June 21, 2015; accepted July 21, 2015. Date of publication August 06, 2015; date of current version nulldate. The guest editor coordinating the review of this manuscript and approving it for publication was XXXXX XXXXXXXXXX.

The authors are with the Department of Electrical and Electronic Engineering, Imperial College London, London SW7 2AZ, U.K. (e-mail: a.manikas@imperial.ac.uk; karen.mak06@imperial.ac.uk).

Color versions of one or more of the figures in this paper are available online at http://ieeexplore.ieee.org.

Digital Object Identifier 10.1109/JSTSP.2015.2465308

I. INTRODUCTION

SELECTION of the Pulse Repetition Frequency (PRF), f_r, of a SAR system plays an important role in preventing range and cross-range ambiguities. For a SISO SAR system, a single beam is employed for transmitting and receiving. In this paper, it is assumed that planar arrays are used to form the required directional beam using beamforming. However other systems, for example a reflector phased array or horn antenna, can be used. The following condition needs to be met to ensure unambiguous returns are received [1]

$$B_D < f_r < \frac{c}{2W_g \sin\theta_i} \tag{1}$$

where c is the speed of light, W_g is the swath width, θ_i is the incident angle and B_D is the Doppler bandwidth defined as the range of Doppler frequencies in the cross-range direction in the antenna footprint [2].

From (1), the condition on the left hand side must be satisfied to prevent cross-range ambiguities by ensuring f_r is greater than B_D. However, f_r cannot be made arbitrarily large, as range ambiguities will occur due to the returns from different transmitted signals overlapping and being received within the same time frame, thus the right hand side of (1) must also be satisfied.

For non-zero squint, B_D is calculated as [2]

$$B_D = \frac{2v}{\lambda}\left(\sin\left(\theta_{sq} + \frac{\lambda}{2L_a}\right) - \sin\left(\theta_{sq} - \frac{\lambda}{2L_a}\right)\right) \tag{2}$$

where θ_{sq} is the squint angle.

In the case of zero squint, i.e., $\theta_{sq} = 0$ (boresight direction), B_D is given as [2], [3]

$$B_D \approx \frac{2v}{L_a} \approx \frac{v_s}{\Delta_{cr}} \tag{3}$$

where $\begin{cases} \Delta_{cr} = & \text{Cross} - \text{range resolution} \\ L_a = & \text{Length of single beamformer} \\ v_s = & \text{Velocity of the SAR system} \end{cases}$

Using (3), (1) becomes

$$\frac{v_s}{\Delta_{cr}} < f_r < \frac{c}{2W_g \sin\theta_i} \tag{4}$$

thus relating the parameters Δ_{cr}, f_r and W_g, indicating that for a fixed value of f_r, an increase in W_g will lead to coarser resolution and vice versa, thus showing that it is not possible to increase both W_g and Δ_{cr} simultaneously resulting in a wide swath, high resolution contradiction.

However in recent years in the field of SAR, there has been considerable interest in so-called multi-channel SAR systems using an array of beamformers and Smart Multi Aperture Radar

Techniques (SMART) SAR systems using an array of beamformers with additional digital beamforming [3]–[6] These allow the above contradiction to be overcome. Of particular interest in this paper are SAR systems with a single transmit beamformer and multiple receive beamformers, which will be referred to as SIMO SAR systems.

In this paper, array processing concepts in communications are applied to SIMO SAR systems, where the aim is to achieve undersampled signal reconstruction. Inspired by the non-uniform displaced phase center sampling algorithm or reconstruction algorithm in [7], shown to be equivalent to null steering in [3], referred to here as the steering vector beamformer, and the superresolution beamformer in [8] for communication systems, a novel superresolution wide null beamformer is proposed for SIMO SAR systems for the reconstruction of the multiple sets of received undersampled signals. The novelty of this algorithm is in the ability to form wide nulls for signal reconstruction and therefore allows the use of a single weight vector for each block of ambiguous Doppler frequencies compared to the existing reconstruction algorithm using a single weight vector for each ambiguous Doppler frequency. As resolution increases as a function of increased aperture length, the proposed beamformer of this SIMO SAR system uses a large aperture, and consequently has increased resolution. Furthermore, the proposed wide null beamformer is also a "subspace" type and thus has infinite (asymptotically) resolution capabilities [9].

Beamforming techniques for SAR systems are first discussed in Section II, before the mathematical modeling of the received signals used throughout this paper is presented in Section III. In particular the modeling of the received signals utilizes the array manifold vector, which is a key concept for the description of the proposed wide null beamformer. Then the proposed beamformer for the formation of wide nulls applied in the Doppler frequency domain for undersampled SAR data reconstruction is presented in Section IV. Representative results are then given in Section V, firstly in a high Signal-to-Noise (SNR) case to allow a better analysis of the capabilities of the proposed beamformer using impulse response cuts of an imaged target. Then a low SNR case with added sea clutter is used for a representative application of the beamformer in a maritime application before this paper concludes in Section VI.

II. Beamforming for SAR Systems

Beamforming algorithms based on subspace techniques are treated extensively in radar applications [10]–[15]. However, with conventional SAR systems employing a single transmit and receive beamformer, referred to here as SISO SAR systems, there is a limitation on the ability to directly apply beamforming algorithms based on subspace techniques [16] due to the need for multiple spatial channels in order to calculate the required covariance matrix. However, by using overlapping subsets of data from a SISO SAR system, subspace techniques can be used to generate higher resolution SAR images [17].

However in recent years, there has been considerable interest in so-called multi-channel SAR systems using an array of beamformers and Smart Multi Aperture Radar Techniques (SMART) SAR systems using an array of beamformers with additional digital beamforming [6]. Applications of these systems include jammer suppression using Space-Time Adaptive Processing (STAP) [18] and clutter suppression. One key area where these systems can be used is in wide swath, high resolution imaging. In the case where a multi-channel SAR system with a single transmit beamformer and K receive beamformers is utilized, referred to here as SIMO SAR systems and with $K > 1$, the single transmit beamformer transmits a chirp signal of duration T seconds, every T_r seconds, resulting in the chirp signal being transmitted a total of N_p times along the flight path. Therefore, due to the design of a SIMO SAR system, K received sets of signals for every transmitted chirp are received, resulting in a total of KN_p samples in the cross-range direction compared to only N_p samples in the case when a SISO SAR system is used.

These additional samples allows (1) to be rewritten for a SIMO SAR system, giving

$$B_D < Kf_r < \frac{c}{2W_g \sin\theta_i} \tag{5}$$

where in comparison to a SISO SAR system

1) in a SIMO SAR system, f_r can be decreased K times while still satisfying (5), resulting in the ability to image a wider swath unambiguously.
2) in a SIMO SAR system, for the same value of f_r, a larger B_D can be used while still satisfying (5), which results in an improved cross-range resolution, as can be seen from (3).

In this paper, point 1 is of interest, where f_r is decreased for each receiver such that (1) is not satisfied resulting in cross-range ambiguities due to undersampling, while allowing the required wide swath width to be imaged. If K beamformers in the cross-range direction are used, (5) can be satisfied, and suppression of these ambiguities or aliases, which correspond to ambiguous Doppler frequencies, can be achieved using array processing techniques to reconstruct a single unaliased output, therefore allowing wide swath, high resolution imaging, compared to SISO SAR systems.

One particular technique to achieve this is the non-uniform displaced phase center sampling algorithm in [7] which, as mentioned in [3], is equivalent to null-steering using the steering vector beamformer, and is given in Appendix A with the notation used throughout this paper. The use of the steering vector beamformer allows the formation of multiple sharp nulls for ambiguous Doppler frequency suppression. However, there are no known examples of using wide nulls for undersampled SAR signal reconstruction in the SAR literature. For this application, the use of wide nulls will allow the suppression of a range of ambiguous Doppler frequencies using a single wide null, compared to multiple sharp nulls. To achieve this, a novel superresolution wide null beamformer for SIMO SAR systems, inspired by the existing non-uniform displaced phase center sampling algorithm in [7] and the superresolution beamformer in [8] for communication systems, is proposed in Section IV.

III. SIMO SAR System Model

A. SIMO SAR Mathematical Modelling

Consider a SIMO SAR system represented in Fig. 1, consisting of a transmitter formed from a planar array of N antenna

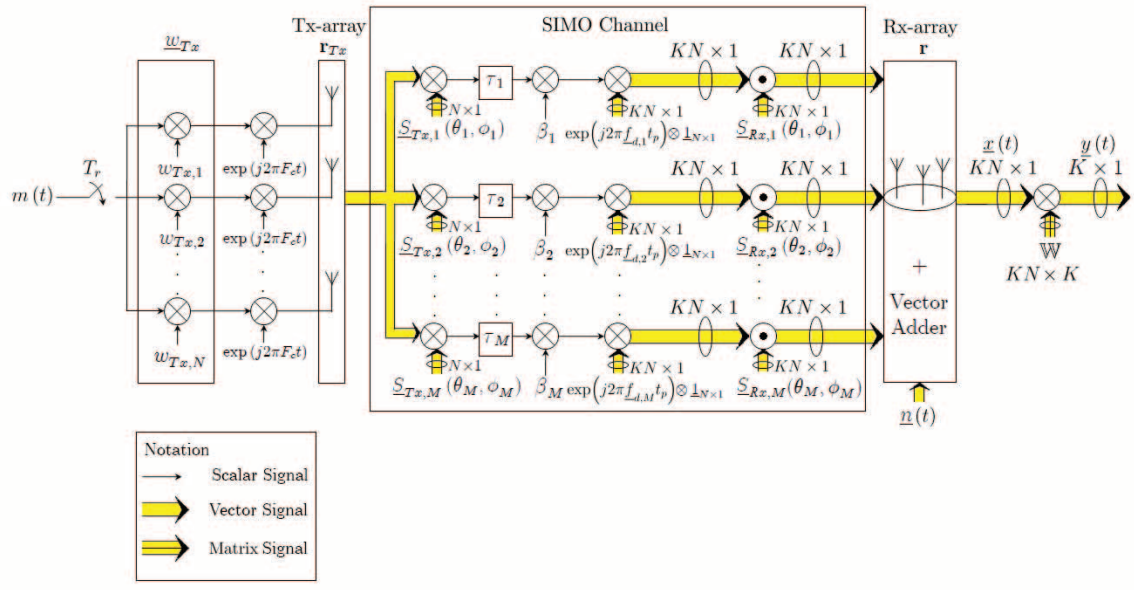

Fig. 1. SIMO SAR system geometry.

elements, which travels along a straight path in the along track direction. The N elements are located on the same platform and have Cartesian coordinates described by the matrix

$$\mathbf{r}_{Tx} = \left[\underline{r}_{Tx,1}, \underline{r}_{Tx,2}, \ldots, \underline{r}_{Tx,N}\right] \tag{6a}$$

$$= \left[\underline{r}_{Tx,x}, \underline{r}_{Tx,y}, \underline{r}_{Tx,z}\right]^T \quad \in R^{3\times N} \tag{6b}$$

where $\underline{r}_{Tx,x}$, $\underline{r}_{Tx,y}$ and $\underline{r}_{Tx,z}$ are $(N \times 1)$ column vectors with the x, y and z coordinates of each transmitter element respectively and $\underline{r}_{Tx,i} \in R^{3\times 1}$ denotes the location of the i^{th} element of the array. Each of the K receive beamformers is also formed using an array of N elements and travels in the direction along the positive x axis, resulting in a total of KN antenna elements, which have Cartesian coordinates described by the matrix

$$\mathbf{r} = [\mathbf{r}_1, \mathbf{r}_2, \ldots, \mathbf{r}_K] \quad \in R^{3\times KN} \tag{7}$$

where $\mathbf{r}_k$ denotes the Cartesian coordinates of the N elements of the k^{th} beamformer defined as

$$\mathbf{r}_k = [\underline{r}_{k,x}, \underline{r}_{k,y}, \underline{r}_{k,z}]^T \quad \in R^{3\times N} \tag{8}$$

with $\underline{r}_{k,x}$, $\underline{r}_{k,y}$ and $\underline{r}_{k,z}$ being column vectors containing the x, y and z coordinates of each element of the k^{th} beamformer respectively. All N elements of each receive beamformer are located on the same platform, however, the K receive beamformers may either be located on the same or separate platforms.

The transmitter, described by the complex $(N \times 1)$ vector $\underline{w}_{Tx}$, produces a single beam and transmits a chirp pulse $m(t)$

$$m(t) = \exp\left(j\pi \frac{B}{T} t^2\right) \tag{9}$$
$$\text{with } t_n < t < t_n + T \text{ for } n = 1, 2, \ldots, N_p$$

where B is the chirp bandwidth and T the chirp pulse duration, with $\frac{B}{T}$ defining the chirp rate.

The scatterers within this beam footprint are illuminated for T seconds and all KN elements of the SIMO SAR system receives the echoes. By assuming a total of M scatterers, the received signal at a particular time t_p can be modeled as a $(KN \times 1)$ vector $\underline{x}(t)$, given as

$$\underline{x}(t) = \sum_{m=1}^{M} \begin{pmatrix} \beta_m \exp(j2\pi f_{d,m} t_p) \\ \cdot \underline{S}_{Rx,m} \underline{S}_{Tx,m}^H \underline{w}_{Tx}[t_n] \\ \cdot m(t - \underline{\tau}_m[t_p]) \end{pmatrix} + \underline{n}(t) \tag{10}$$

with $p = 1, 2, \ldots, N_p$ and $n = 1, 2, \ldots, N_p$, where a chirp transmitted at t_n is received at $t_p \leqslant t \leqslant t_p + \frac{2(R_f - R_n)}{c} + T$

with
- β_m = Complex number containing various constants associated with the m^{th} scatterer, for example scatterer reflectivity and path gain.
- (θ_m, ϕ_m) = (azimuth, elevation) angle associated with the m^{th} scatterer with reference to $(0, 0, 0)$.
- $\underline{\tau}_m[t_p]$ = $(KN \times 1)$ vector of Round trip delays associated with the m^{th} scatterer.
- ρ_m = Slant range between m^{th} scatterer and $(0, 0, 0)$.
- $n(t)$ = Noise.
- $\underline{w}_{Tx}$ = $(N \times 1)$ weight vector of the N antenna elements of the single beamformer forming the transmit beam.
- $f_{d,m}$ = Doppler frequency shift associated with the m^{th} scatterer.
- R_f = Far slant range.
- R_n = Near slant range.
- $\underline{S}_{Rx,m}$ = $(KN \times 1)$ receiver array manifold vector associated with the m^{th} scatterer.
- $\underline{S}_{Tx,m}$ = $(N \times 1)$ transmitter array manifold vector associated with the m^{th} scatterer.

The $(N \times 1)$ complex vector $\underline{S}_{Tx,m}$ is the transmitter array manifold vector associated with the m^{th} scatterer described as

$$\underline{S}_{Tx,m} \triangleq \underline{S}_{Tx}\left(\mathbf{r}_{Tx}[t_n], \theta_m, \phi_m, \rho_m\right) \tag{11a}$$

$$= \rho_m^a \odot \underline{R}_{Tx,m}^{-a}[t_n] \odot \exp\left(+j\frac{2\pi F_c}{c}\left(\rho_m \cdot \underline{1}_N - \underline{R}_{Tx,m}[t_n]\right)\right) \tag{11b}$$

with

$$\underline{R}_{Tx,m}[t_n] = \sqrt{\rho_m^2 \cdot \underline{1}_N + \underline{r}_{Tx,x}^2[t_n] + \underline{r}_{Tx,y}^2[t_n] + \underline{r}_{Tx,z}^2[t_n] - \frac{\rho_m c}{\pi F_c}\mathbf{r}_{Tx}^T[t_n]\underline{k}\left(\theta_m, \phi_m\right)} \tag{12}$$

where ρ_m is the reference slant range between the SAR system and the m^{th} scatterer, a is the path loss exponent and $\underline{k}\left(\theta_m, \phi_m\right)$ is the wavenumber vector given as

$$\underline{k}\left(\theta_m, \phi_m\right) = \frac{2\pi F_c}{c}\begin{bmatrix}\cos(\theta_m)\cos(\phi_m)\\ \sin(\theta_m)\cos(\phi_m)\\ \sin(\phi_m)\end{bmatrix} \tag{13a}$$

$$= \frac{2\pi F_c}{c}\underline{u}(\theta_m, \phi_m) \tag{13b}$$

and $\underline{u}\left(\theta_m, \phi_m\right)$ is a (3×1) unit vector pointing in the direction (θ_m, ϕ_m) of the m^{th} scatterer.

Similarly the $(KN \times 1)$ complex vector $\underline{S}_{Rx,m}$ is the receiver array manifold vector associated with the m^{th} scatterer described as

$$\underline{S}_{Rx,m} \triangleq \underline{S}_{Rx}\left(\mathbf{r}[t_p], \theta_m, \phi_m, \rho_m\right) \tag{14a}$$

$$= \rho_m^a \odot \underline{R}_m^{-a}[t_p] \odot \exp\left(-j\frac{2\pi F_c}{c}\left(\rho_m \cdot \underline{1}_{KN} - \underline{R}_m[t_p]\right)\right) \tag{14b}$$

with

$$\underline{R}_m[t_p] = \sqrt{\rho_m^2 \cdot \underline{1}_N + \underline{r}_x^2[t_p] + \underline{r}_y^2[t_p] + \underline{r}_z^2[t_p] - \frac{\rho_m c}{\pi F_c}\mathbf{r}^T[t_p]\underline{k}(\theta_m, \phi_m)} \tag{15}$$

and where the difference in signs in $\underline{S}_{Tx,m}$ and $\underline{S}_{Rx,m}$ is due to the opposite flow of energy between transmitting and receiving.

In the case when the m^{th} scatterer is located in the far field of the beamformer, i.e., ρ_m is much greater than the array's real aperture, (11) and (14) reduce to the plane wave propagation manifold vector expressed as

$$\underline{S}_{Tx,m} = \exp\left(+j\mathbf{r}_{Tx}^T[t_n]\underline{k}\left(\theta_m, \phi_m\right)\right) \tag{16}$$

and

$$\underline{S}_{Rx,m} = \exp\left(-j\mathbf{r}^T[t_p]\underline{k}\left(\theta_m, \phi_m\right)\right) \tag{17}$$

Using the manifold vector, the $(N \times 1)$ weight vector $\underline{w}_{Tx}$, given in (18) is designed such that a single beam is formed whose mainlobe points in the direction $(\theta_c[t_n], \phi_c[t_n])$ for all t_n, with $n = 1, 2, \ldots, N_p$, where $\theta_c[t_n]$ and $\phi_c[t_n]$ are the azimuth and elevation angles between the center of the beam footprint on the ground respectively

$$\underline{w}_{Tx}[t_n] = \underline{S}_{Tx}\left(\mathbf{r}_{Tx}[t_n], \theta_c[t_n], \phi_c[t_n]\right) \tag{18}$$

where the required data collection mode determines the time dependency on t_n. Examples of data collection modes include Stripmap, ScanSAR, Spotlight, and TOPSAR (Terrain Observation by Progressive Scans).

Likewise, the KN elements of the system forming the K receive beamformers are weighted such that K beams are formed to receive the scatterer echoes. The $(KN \times K)$ weight matrix $\mathbb{W}[t_p]$ is described by

$$\mathbb{W}[t_p] = \begin{bmatrix}\underline{w}_1[t_p], & \underline{0}_{N\times 1}, & \cdots & \underline{0}_{N\times 1}\\ \underline{0}_{N\times 1}, & \underline{w}_2[t_p], & \cdots & \underline{0}_{N\times 1}\\ \vdots & \vdots & \ddots & \vdots\\ \underline{0}_{N\times 1}, & \underline{0}_{N\times 1}, & \cdots & \underline{w}_K[t_p]\end{bmatrix} \tag{19}$$

where $\underline{w}_k[t_p]$ is an $(N \times 1)$ vector of the weights of the N elements of the k^{th} beamformer at time t_p given by

$$\underline{w}_k[t_p] = \underline{S}_{Rx}\left(\mathbf{r}_k[t_p], \theta_c[t_p], \phi_c[t_p]\right) \tag{20}$$

Due to the assumption that the N antenna elements forming a single beam are collocated, the round trip delay between the elements and the m^{th} scatterer can be described by $\frac{2R_m[t_p]}{c}$. However, all K groups of N elements may not be collocated and may be located on different platforms. Therefore the round trip delays will differ. As a result, it can be described by the $(KN \times 1)$ vector $\underline{\tau}_m[t_p]$ given as

$$\underline{\tau}_m[t_p] = \begin{bmatrix}\frac{R_{Tx,m}[t_n]+R_{Rx,1,m}[t_p]}{c} \cdot \underline{1}_N\\ \frac{R_{Tx,m}[t_n]+R_{Rx,2,m}[t_p]}{c} \cdot \underline{1}_N\\ \cdots\\ \frac{R_{Tx,m}[t_n]+R_{Rx,K,m}[t_p]}{c} \cdot \underline{1}_N\end{bmatrix} \tag{21a}$$

$$= \begin{bmatrix}\frac{2\rho_m+\Delta R_{Tx,m}[t_n]+\Delta R_{Rx,1,m}[t_p]}{c} \cdot \underline{1}_N\\ \frac{2\rho_m+\Delta R_{Tx,m}[t_n]+\Delta R_{Rx,2,m}[t_p]}{c} \cdot \underline{1}_N\\ \cdots\\ \frac{2\rho_m+\Delta R_{Tx,m}[t_n]+\Delta R_{Rx,K,m}[t_p]}{c} \cdot \underline{1}_N\end{bmatrix} \tag{21b}$$

where $R_{Tx,m}[t_n]$ and $R_{Rx,k,m}[t_p]$ are the slant ranges between the transmit beamformer and the m^{th} scatterer and the k^{th} receive beamformer and m^{th} scatterer, and $\Delta R_{Tx,m}[t_n]$ and $\Delta R_{Rx,k,m}[t_p]$ are the differences between $R_{Tx,m}[t_n]$ and $R_{Rx,k,m}[t_p]$ with the reference slant range ρ_m for n and $p = 1, 2, \ldots, N_p$ and where a chirp signal transmitted at time t_n is received at time t_p.

The K receiver array output can then be modeled as

$$\underline{y}(t) = \sum_{m=1}^{M}\begin{pmatrix}\beta_m \exp\left(j2\pi \underline{f}_{d,m} t_p\right)\\ \odot\left(\mathbb{W}\left[t_p\right]^H \underline{S}_{Rx,m}\right) \cdot \underline{S}_{Tx,m}^H \underline{w}_{Tx}[t_n]\\ \cdot m\left(t - \underline{\tau}_m\left[t_p\right]\right)\end{pmatrix} + \underline{n}(t) \tag{22}$$

with $p = 1, 2, \ldots, N_p$ and $n = 1, 2, \ldots, N_p$, where a chirp transmitted at t_n is received at $t_p \leqslant t \leqslant t_p + \frac{2(R_f - R_n)}{c} + T$, and where the k^{th} element of $\underline{y}(t)$ corresponds to the signals received by the k^{th} receive beamformer and $\underline{\tau}[t_p]$ is now a $(K \times 1)$ vector of round trip delays associated with the m^{th} scatterer and K beamformers and

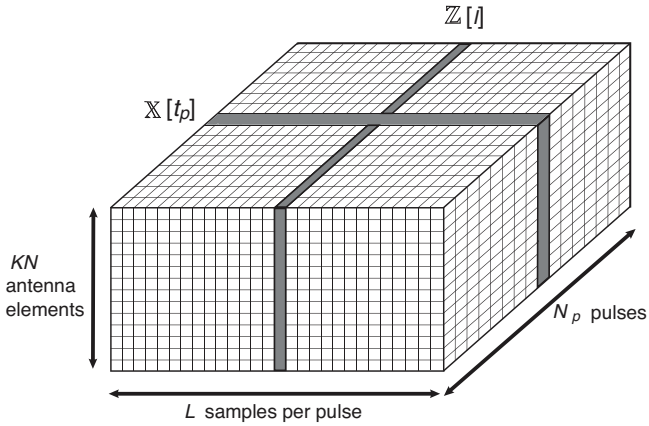

Fig. 2. 3D datacube of the received signals at all KN elements of the SIMO SAR system after discretisation.

$$\text{where} \begin{cases} \mathbb{W}(t_p) & = & (KN \times K) \text{ matrix of the weights of the elements of the } K \text{ receive beamformers.} \\ \underline{f}_{d,m} & = & (K \times 1) \text{ vector of the Doppler frequency shifts associated with the } m^{th} \text{ scatterer and } K \text{ beamformers.} \end{cases}$$

When all K receivers are on the same platform, planewave propagation can be assumed, but when they are located on different platforms, the spherical wave propagation manifold vector should be utilized. However, the elements of the manifold vector that are on the same platform will have approximately equal ranges thus collapsing to the planewave propagation manifold vector.

B. Discrete Time Modelling

The received signals at the KN array elements of the SIMO SAR system are sampled at a sampling rate of F_s to obtain L samples and the discrete samples can be represented by a 3D datacube, shown in Fig. 2, where $\mathbb{X}[t_p]$ is a $(KN \times L)$ matrix describing the data received at all KN elements of the SIMO SAR system, given as

$$\mathbb{X}[t_p] = [\underline{x}[1, t_p], \underline{x}[2, t_p], \ldots, \underline{x}[L, t_p]] \tag{23}$$

with $\underline{x}[l, t_p]$ being the l^{th} sample of the vector $\underline{x}(t)$ at time t_p. $\mathbb{Z}[l]$ is a $(KN \times N_p)$ matrix describing the data received at all KN antenna elements at a particular sample at l.

Weights are then designed and applied to all KN elements to form K outputs, i.e., beams, resulting in a $(K \times N_p \times L)$ datacube, as shown in Fig. 3.

Here $\mathbb{Y}[k]$ is an $(L \times N_p)$ matrix containing all the data received by the k^{th} beamformer from all N_p transmitted chirp pulses and matrix $\overline{\mathbb{X}}[t_p]$ is a $(K \times L)$ matrix describing the data received by the K beamformers and is modeled as

$$\overline{\mathbb{X}}[t_p] = \sum_{m=1}^{M} \begin{pmatrix} \beta_m \exp\left(j2\pi \underline{f}_{d,m} t_p\right) \\ \odot diag\left\{\mathbb{W}[t_p]^H (\underline{S}_{Rx,m})\right\} \underline{S}_{Tx,m}^H \underline{w}_{Tx}[t_n] \\ \cdot \mathbb{M}_m[t_p] \end{pmatrix} + \mathbb{N}[t_p] \tag{24}$$

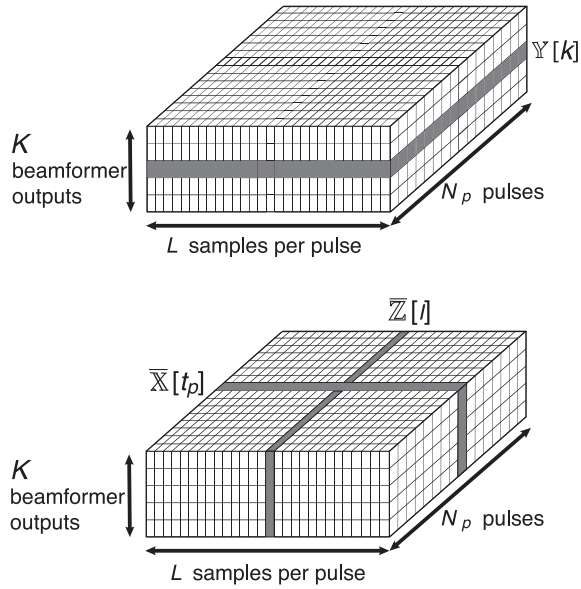

Fig. 3. The outputs of the K receiver beamformers after discretisation in the range direction.

where

$$\mathbb{M}_m[t_p] = \begin{bmatrix} \left(\mathbb{J}^{\tau_{m,1}[t_p]} \underline{m}\right)^T \\ \left(\mathbb{J}^{\tau_{m,2}[t_p]} \underline{m}\right)^T \\ \cdots \\ \left(\mathbb{J}^{\tau_{m,K}[t_p]} \underline{m}\right)^T \end{bmatrix} \tag{25}$$

$$\text{with} \begin{cases} \tau_{m,k}[t_p] & = & \text{Round trip delay associated with the } m^{th} \text{ scatterer from the transmit beamformer to the } k^{th} \text{ receive beamformer at time } t_p. \\ \underline{m} & = & \text{Discretised transmitted chirp pulse of length } T \cdot F_s \text{ samples zero padded with } L - \lceil T \cdot F_s \rceil \text{ zeros.} \\ \mathbb{J} & = & \begin{bmatrix} \underline{0}_{L-1}^T & 0 \\ \mathbb{I}_{L-1} & \underline{0}_{L-1} \end{bmatrix} \\ & = & (L \times L) \text{ shifting matrix.} \\ \mathbb{N}[t_p] & = & (K \times L) \text{ noise matrix.} \end{cases}$$

The $(K \times N_p)$ matrix $\overline{\mathbb{Z}}[l]$ describes the data received by the array of K receivers at a particular range sample at l and can be seen as a range sample spacetime snapshot. Similarly $\overline{\mathbb{X}}[t_p]$ can be seen as a cross-range sample spacetime snapshot, with the t_p^{th} pulse being analogous to the t_p^{th} cross range sample.

IV. Superresolution Wide Null Beamforming

Aliasing of the spectrum of the received signals in the cross-range direction occurs due to undersampling when (1) is not satisfied. Therefore suppression of the ambiguities is required in order to allow the reconstruction of the full Doppler spectrum over the frequencies $-\frac{Kf_r}{2}$ to $+\frac{Kf_r}{2}$, where each beamformer receives a section of the Doppler bandwidth. For the k^{th}receiver this is defined as being over the range [3]

$$f_{d,k} = \left[\left(-\frac{K}{2} + k - 1\right) f_r, \left(-\frac{K}{2} + k\right) f_r\right] \tag{26}$$

for $k = 1, 2, \ldots, K$.

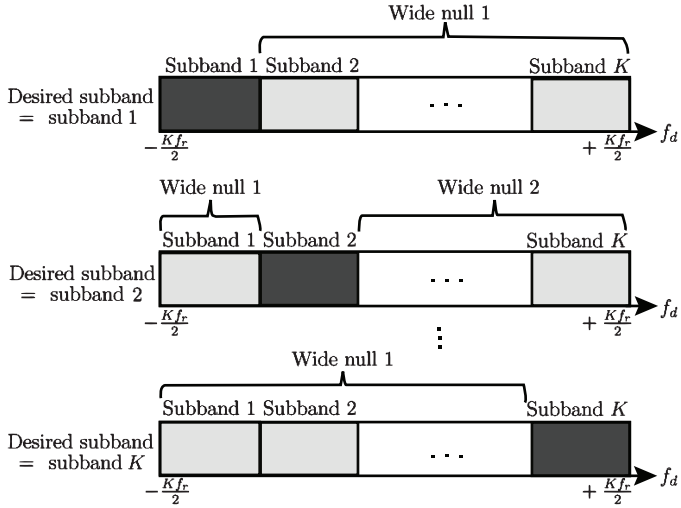

Fig. 4. Representation of suppression of subbands, where the dark grey subbands are desired.

Fig. 4 gives a representation of these frequency ranges, defined as subbands, where the aim is to reconstruct the full Doppler frequency range from $-\frac{Kf_r}{2}$ to $+\frac{Kf_r}{2}$. By identifying the desired subbands, shown in dark grey in Fig. 4, and suppressing all other ambiguous subbands, reconstruction using array processing techniques is possible, where for the k^{th} receiver beamformer, the ambiguous Doppler frequencies cover all $f_{d,i}$ for $i \neq k$, with $k = 1, 2, \ldots, K$. With reference to Fig. 4, it can be seen that a wide null could be designed such that $\geqslant 1$ ambiguous subbands is suppressed at a time. In this case, only up to two wide nulls need to be formed at a time without suppressing the desired subband, where two nulls, $M_b = 2$, are required when $K > 2$ and only one null, $M_b = 1$, is required if $K = 2$.

By first considering the formation of a single wide null, the $(K \times K)$ matrix $\mathbb{Q}_I$ for the ambiguous Doppler frequency range $f_{d,I}$ can be calculated as

$$\mathbb{Q}_I = \int \underline{S}_{I,b}\left(f_d\right) \underline{S}_{I,b}^H\left(f_d\right) df_{d,I} \tag{27}$$

which can be seen as the summation of $\underline{S}_{I,b}(f_d)\underline{S}_{I,b}^H(f_d)$ for all f_d within the range $f_{d,I}$, with $\underline{S}_{I,b}(f_d)$ being the manifold vector in terms of Doppler frequency, described by (29) where the subscript I, b is used here to indicate the Doppler frequency at which the manifold vector is calculated at is to be suppressed. As it is assumed that the K receiver beamformers form a linear array along the positive x axis and

$$f_d = \frac{2v}{\lambda}\sin(\theta_{sq}) \tag{28a}$$

$$= \frac{2v}{\lambda}\cos(\theta)\cos(\phi) \tag{28b}$$

with θ_{sq} being the squint angle, the manifold vector $\underline{S}(\theta, \phi)$ can be represented in terms of Doppler frequency and simplified to give

$$\underline{S}(f_d) = \begin{cases} \exp\left(-j\frac{\pi}{v}\underline{r}_x[0]f_d\right) \\ \text{for plane wave propagation} \\ \rho_c(f_d)^a \odot \underline{R}(f_d)^{-a} \\ \odot \exp\left(-j\frac{2\pi}{\lambda}\left(\rho_c(f_d)\cdot \underline{1}_K - \underline{R}(f_d)\right)\right) \\ \text{for spherical wave propagation} \end{cases} \tag{29}$$

where $\underline{r}_x[0]$ is a $(K \times 1)$ vector of the x coordinates of the center element of the K beamformers at time $t_p = 0$ and ρ_c is the slant range to the center of the beam footprint and

$$\underline{R}(f_d) = \sqrt{\rho_c^2(f_d)\cdot \underline{1}_K + \underline{r}_x^2[0] - \frac{\rho_c(f_d)\lambda}{v}\underline{r}_x[0]f_d} \tag{30}$$

By forming the $(K \times \tau_I)$ matrix

$$\mathbb{E}_I = [\underline{E}_{I,1}, \underline{E}_{I,2}, \ldots, \underline{E}_{I,\tau_I}] \tag{31}$$

where $\underline{E}_{I,j}$ is the j^{th} eigenvector of $\mathbb{Q}_I$, with τ_I satisfying the condition

$$\sum_{k=\tau_I+1}^{K} \lambda_{I,k} \leqslant \gamma \tag{32}$$

where $\lambda_{I,k}$ is the k^{th} eigenvalue of $\mathbb{Q}_I$ and $-10\log_{10}\gamma$ is a defined threshold in dBs giving the level of suppression[1], and then calculating its complement projection to give $\mathbb{P}_{\mathbb{E}_I}^{\perp}$

$$\mathbb{P}_{\mathbb{E}_I}^{\perp} = \mathbb{I}_K - \left(\mathbb{E}_I\left(\mathbb{E}_I^H\mathbb{E}_I\right)^{-1}\mathbb{E}_I^H\right) \tag{33}$$

a $(K \times 1)$ weight vector is formed, such that after performing $\mathbb{P}_{\mathbb{E}_I}^{\perp}\underline{S}_d(f_d)$ a wide null is formed over the Doppler frequency range $f_{d,I}$. $\underline{S}_d(f_d)$ is the manifold vector at the desired Doppler frequency assumed to be the center Doppler frequency of the desired subband[2], and is calculated as

$$f_{d,c} = \left(-\frac{K}{2} + k - \frac{1}{2}\right) f_r \tag{34}$$

for the k^{th} beamformer, with $k = 1, 2, \ldots, K$.

In the general case where M_b wide nulls are required, the above technique can be extended by forming the matrix $\mathbb{S}_I$

$$\mathbb{S}_I = [\mathbb{E}_{I,1}, \mathbb{E}_{I,2}, \ldots, \mathbb{E}_{I,M_b}] \tag{35}$$

and calculating its complement projection $\mathbb{P}_{\mathbb{S}_I}^{\perp}$ to give the required weights, which when normalized is given as

$$\underline{w} = \frac{\mathbb{P}_{\mathbb{S}_I}^{\perp}\cdot \underline{S}_d}{\sqrt{\underline{S}_d^H \cdot \mathbb{P}_{\mathbb{S}_I}^{\perp}\cdot \underline{S}_d}} \tag{36}$$

By evaluating the required $(K \times 1)$ weight vector $\underline{w}$ for all K subbands, the reconstructed data can be represented as

$$\mathbb{Y}_{recon} = \left[\underline{w}_{\mathbb{I},1}^T \cdot \mathbb{X}_{concat}, \underline{w}_{\mathbb{I},2}^T \cdot \mathbb{X}_{concat}, \ldots, \underline{w}_{\mathbb{I},K}^T \cdot \mathbb{X}_{concat}\right]^T \tag{37}$$

where $\underline{w}_{\mathbb{I},k} = (\mathbb{I}_{N_p} \otimes \underline{w}_k)$ for $k = 1, 2, \ldots, K$ and

$$\mathbb{X}_{concat} = \begin{bmatrix} \overline{\mathbb{X}}[1] \\ \overline{\mathbb{X}}[2] \\ \vdots \\ \overline{\mathbb{X}}[N_p] \end{bmatrix} \tag{38}$$

[1]Note that the value γ can take is also limited by the number of receive beamformers. With K beamformers, there are only $(K-1)$ values γ can take. Likewise this results in only $(K-1)$ possible values of τ_I. The effect of K on γ and τ_I selection is discussed in Appendix B.

[2]This results in the center of the mainlobe of the beamformer to be at the center Doppler frequency of the desired subband and therefore resulting in a symmetrical response.

where $\overline{\mathbb{X}}[n_p]$ is the data at the n_p^{th} range line in the range Doppler domain and $\underline{w}_k$ is the required weight vector for suppression of all subbands other than the k^{th} subband for $k = 1, 2, \ldots, K$.

As mentioned in [3], when the K receivers are sparsely located in space, the increased separation between the transmitter and receiver may need to be taken into account with additional phase terms. In the case of $K = 2$, these extra terms can be combined with the calculated weights as follows

$$\mathbb{W} = diag \left\{ \begin{array}{c} \exp\left(+j\frac{(r_{x,1}[0])^2}{2\lambda R_o}\right) \\ \exp\left(+j\frac{(r_{x,2}[0])^2}{2\lambda R_o}\right) \end{array} \right\} \mathbb{W}_K \tag{39}$$

where $\mathbb{W}_K = [\underline{w}_1, \underline{w}_2, \ldots, \underline{w}_K]$.

Also, due to an increased distance between the receivers, the range history of a single scatterer can no longer be assumed approximately equal at all K receivers. Therefore this difference in range history between receivers needs to be compensated. In order to compensate for this, a range shift must be applied before the superresolution beamformer to ensure that the range history of the imaged scatterers are approximately similar in all K sets of data. From [3], a shift related to distances between each receive beamformer and a reference slant range can be applied. By assuming the center element of the first beamformer of the array of K beamformers is the reference, the required shift required for the k^{th} beamformer can be applied using (40) and (41).

with
- $F_{\text{col}}(\mathbb{A})$ = Fourier transform performed down each column of matrix $\mathbb{A}$.
- $F_{\text{col}}^{-1}(\mathbb{A})$ = Inverse Fourier transform performed down each column of matrix $\mathbb{A}$.
- $\underline{f}_{sr}$ = $(L \times 1)$ vector of indices of the frequencies in the slant range direction.
- $\underline{R}_k[t_p]$ = $(L \times 1)$ vector of indices of the slant ranges and the center element of the k^{th} beamformer at time t_p.

Algorithm Summary

1) Apply range compression on to the K sets of data: $\mathbb{Y}_1$, $\mathbb{Y}_2, \ldots, \mathbb{Y}_K$, which when stacked to form a $(K \times L \times N_p)$ datacube, allows the $(K \times L)$ matrix $\overline{\mathbb{X}}[f_d]$ to be extracted for all Doppler frequencies, where $\overline{\mathbb{X}}[f_d]$ is $\overline{\mathbb{X}}[t_p]$ (see Fig. 3) in the Doppler frequency domain.
2) Ensure that the processed sets of data are in the range-Doppler domain. In the case where a sparse array of K receiver beamformers is used, apply additional compensation to ensure that the range histories of the same target between the K sets of received data are approximately equal using (40).
3) Identify the range of frequencies within all K subbands using (26).
4) Identify the center Doppler frequency of all K subbands using (26), and for the desired subband form the manifold vector, $\underline{S}_d(f_d)$ for the desired Doppler frequency, which is assumed to be the center Doppler frequency of the desired band.
5) For the formation of a wide null, identify the ambiguous Doppler frequencies to be suppressed, where for the k^{th} receiver's data, the ambiguous Doppler frequency ranges are calculated from (26) for $i \neq k$. Form the $(M_b \times 1)$ manifold vector $\underline{S}_{I,b}(f_d)$ for each wide null and find the τ_I most significant eigenvalues, $\mathbb{E}_{I,b}$, from the matrix $\mathbb{Q}_I$ using (27) and form the matrix $\mathbb{S}_I$ using (35).
6) Form the $(K \times 1)$ weight vector $\underline{w}_k$, for $k = 1, 2, \ldots, K$ using (36) and if required, apply extra phase terms to take into account sparse arrays.
7) Apply the weights, $\underline{w}_1$, $\underline{w}_2, \ldots,$ $\underline{w}_K$, to $\mathbb{X}_{concat}$ formed using (38), to obtain the reconstructed data using (37).
8) Continue with any further steps in the image formation algorithm of choice to form a single focused image with reduced cross-range ambiguities.

V. Results

In this section, the performance of the proposed superresolution beamformer will be analyzed for a collocated array of K receiver beamformers such that it can be assumed the range histories of M_d imaged targets of interest are approximately equal between the K sets of received data. The superresolution beamformer is integrated into the Chirp Scaling Algorithm to form a focused image from the K sets of undersampled received data. Based on typical airborne parameters given in [19], the simulation parameters in Table I are used[3], where $K = 2$ has been chosen as this is a common SIMO SAR system configuration and examples of the application of beamforming for the suppression of cross-range ambiguities in existing systems are available [20], [21].

To show the capabilities of the proposed beamformer, two cases will be presented:

1) A high SNR case of 30 dB, where $M_d = 1$. Although this will not be true in practice, this will allow better analysis of the resulting Impulse Response Functions (IRF) of the imaged target and capabilities of the proposed beamformer without the target's alias being 'covered' by noise and surrounding clutter.
2) A low SNR case of -30 dB, where $M_d > 1$ with sea clutter. This will allow the capabilities of the proposed

[3]The designed parameters provide a trade-off between simulation time and actual airborne SAR imaging geometry parameters.

$$F_{\text{col}}^{-1}\left(F_{\text{col}}(\mathbb{Y}_k) \odot \exp\left(-j2\pi \cdot \left(\underline{f}_{sr} \cdot \underline{1}_{N_p \times 1} \odot \Delta\mathbb{R}_k \odot \Delta\mathbb{R}_k\right)\right)\right) \tag{40}$$

$$\Delta\mathbb{R}_k = \left[\underline{R}_k[t_1], \underline{R}_k[t_2], \ldots, \underline{R}_k\left[t_{N_p}\right]\right] - \left[\underline{R}_1[t_1], \underline{R}_1[t_2], \ldots, \underline{R}_1\left[t_{N_p}\right]\right] \tag{41}$$

TABLE I
SIMULATION PARAMETERS FOR UNDERSAMPLING RECONSTRUCTION

h	Altitude	10.0	km
f_r	Pulse Repetition Frequency	300.0	Hz
B	Chirp bandwidth	100.0	MHz
B_d	Doppler bandwith	433.0	Hz
F_c	Carrier frequency	9.4	GHz
K	Number of receive beamformers	2.0	
R_f	Far slant range	34.2	km
R_n	Near slant range	25.6	km
T	Chirp length	10.0	μs
V_s	Platform velocity	250.0	ms^{-1}

TABLE II
IMAGED TARGET PARAMETERS AND IMAGE SAMPLE LOCATIONS

Target 1	
$r_{m,x}$ (m)	300.00
ρ_m (m)	25694.75
θ_m $(^o)$	89.27
ϕ_m $(^o)$	22.90
In image from undersampled data	
Expected slant range image sample	81.00
Expected cross-range image sample	361.00
In image from reconstructed data	
Expected slant range image sample	81.00
Expected cross-range image sample	722.00

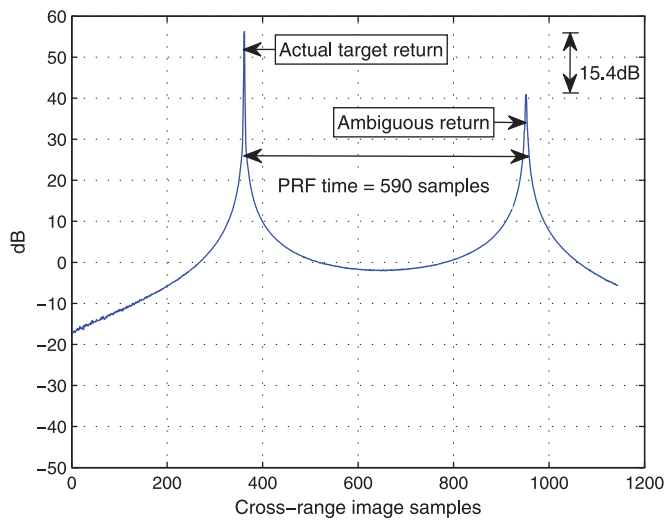

Fig. 5. Log slant range cut of image from undersampled received data.

beamformer to be seen from the formed image after beamforming in a representative maritime environment.

In both cases the proposed wide null beamformer performance will be compared and analyzed with the steering vector beamformer detailed in Appendix A. As mentioned in [3], in the case of K collocated beamformers, the steering vector beamformer is equivalent to the non-uniform displaced phase center sampling technique described in [7].

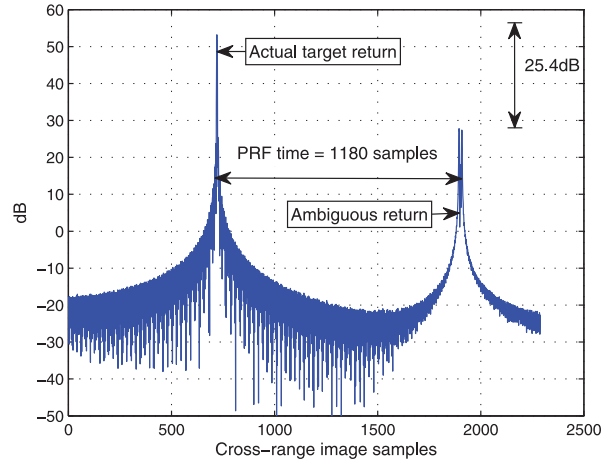

Fig. 6. Log slant range cut of reconstructed image using steering vector beamformer.

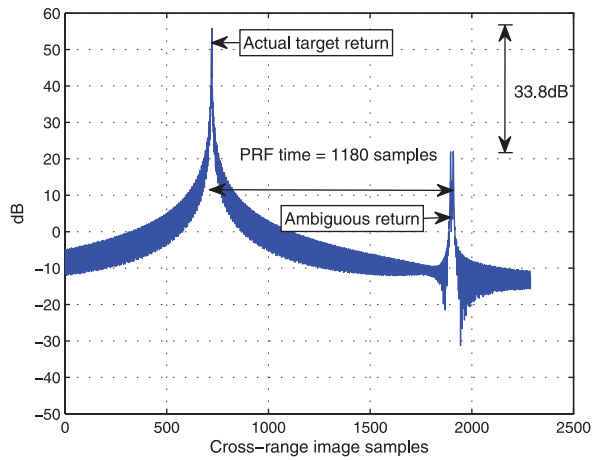

Fig. 7. Log slant range cut of reconstructed image using proposed wide null beamformer.

A. Case 1: $M_d = 1$ With no Clutter

In this case a single target is simulated with parameters given in Table II and with added noise in the imaging environment at a high SNR of 30 dB to better illustrate the effect of proposed beamformer before and after processing and to show the location of the ambiguities to be suppressed.

By plotting cuts at a specific slant range sample number, i.e., range gate corresponding to the target in the formed SAR image, the Impulse Response Function (IRF) of the imaged target can be analyzed. As undersampled raw data is used, it is important to know the location of the ambiguous returns of a particular target in the image space. These locations are related to the PRF time given as [19]

$$\Delta T_r \approx \frac{cR_m(t_p)f_r}{2F_cV_s^2\cos^2(\theta_{sq,m})} \tag{42}$$

Due to the sampling in the cross range direction by f_r, the ambiguous returns will occur at samples which are integer multiples of $f_r\Delta T_r$ to the left and right of the actual target response. With reference to Fig. 5, which is a slant range cut of the focused image of the undersampled raw data received at beamformer 1, it can be seen that although a single target was imaged, its ambiguous return is clearly visible $f_r\Delta T_r$ samples away from the actual target return. The peak-to-ambiguity ratio, i.e., the ratio

TABLE III
IMAGED TARGET PARAMETERS AND IMAGE SAMPLE LOCATIONS

	Target 1	Target 2	Target 3	Target 4	Target 5	Target 6	Target 7	Target 8
$r_{m,x}$ (m)	300.00	309.00	300.00	309.00	296.00	100.00	102.00	200.00
ρ_m (m)	25694.75	25694.86	25688.75	25688.86	25691.71	25633.20	25638.20	25793.78
θ_m $(^o)$	89.27	89.25	89.27	89.25	89.28	89.76	89.75	89.52
ϕ_m $(^o)$	22.90	22.90	22.91	22.91	22.91	22.96	22.96	22.81
In image from undersampled data								
Expected slant range image sample	81.00	81.00	76.00	76.00	79.00	33.00	37.00	16.00
Expected cross-range image sample	361.00	372.00	361.00	372.00	356.00	121.00	124.00	241.00
In image from reconstructed data								
Expected slant range image sample	81.00	81.00	76.00	76.00	79.00	33.00	37.00	16.00
Expected cross-range image sample	722.00	744.00	722.00	744.00	712.00	242.00	247.00	482.00

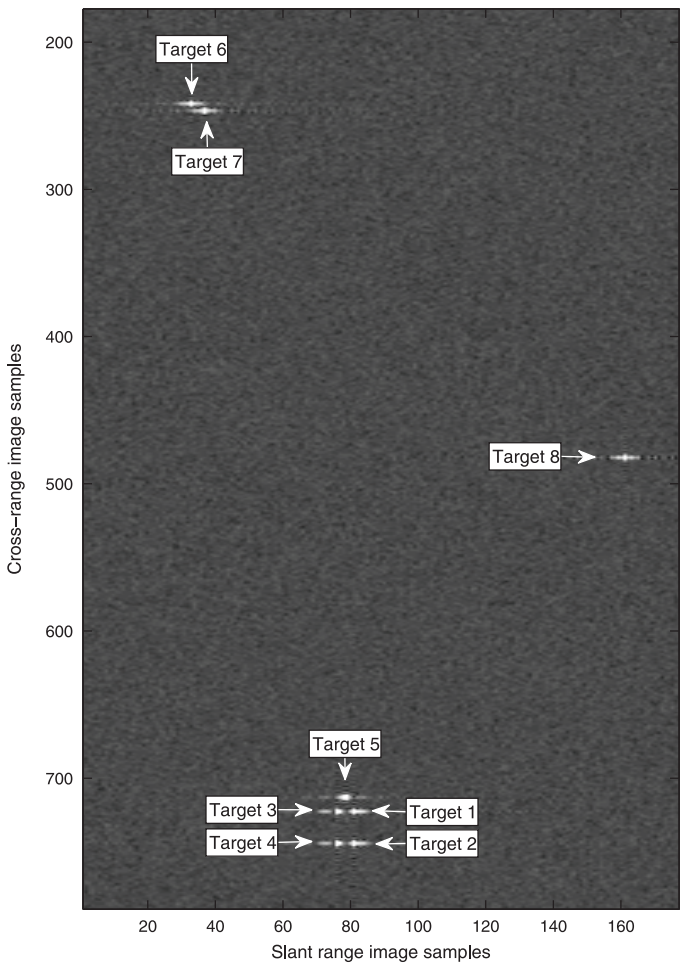

Fig. 8. Focused image, using a single receive beamformer, of imaged targets with locations given in Table III, when no undersampling occurs.

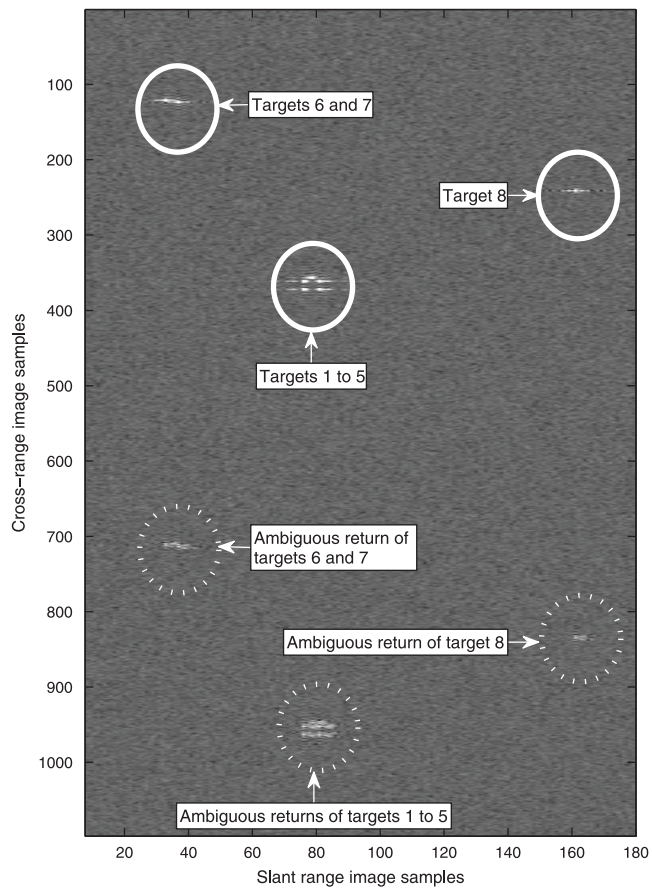

Fig. 9. Focused image from undersampled received data.

of the actual target return and its ambiguous replica is about 15.4 dB.

However, by making use of the $K = 2$ sets of undersampled data, the steering vector beamformer described in Appendix A allows suppression of the ambiguous returns and reconstruction of the two sets of undersampled data. The improvement can be seen in Fig. 6, where although the ambiguous replica is still present, its response has been suppressed, increasing the peak-to-ambiguity ratio from 15.4 dB to about 25.4 dB. However, in a practical scenario this ambiguity response may be 'covered' by noise and surrounding clutter and therefore may not be visible in the formed SAR image.

Instead of the steering vector beamformer, the use of the proposed wide null beamformer applied to the $K = 2$ sets of undersampled data results in Fig. 7. Like the case when the steering vector beamformer is applied, the ambiguous replica is suppressed but still present. However, in practical scenarios the replica may be 'covered' by noise and surrounding clutter making it less visible in the formed SAR image. Here there is an improvement in the peak-to-ambiguity ratio from 25.4 dB to about 33.8 dB compared to the steering vector beamformer.

The 3 dB width of the target's IRF, i.e., cross-range resolution, in both the steering vector beamformer and proposed beamformer is also improved compared to when no reconstruction

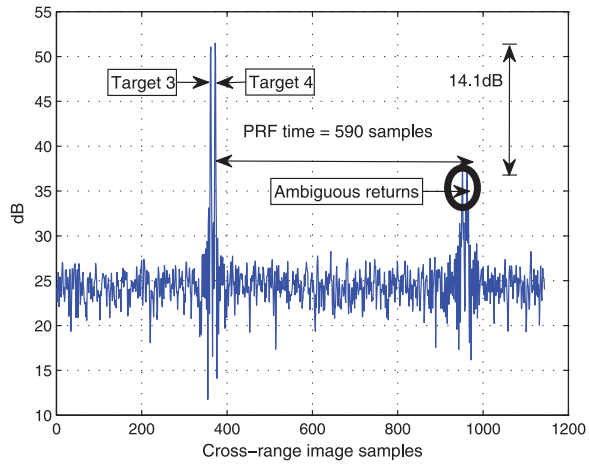

Fig. 10. Log slant range cut of image formed from undersampled received data across targets 3 and 4.

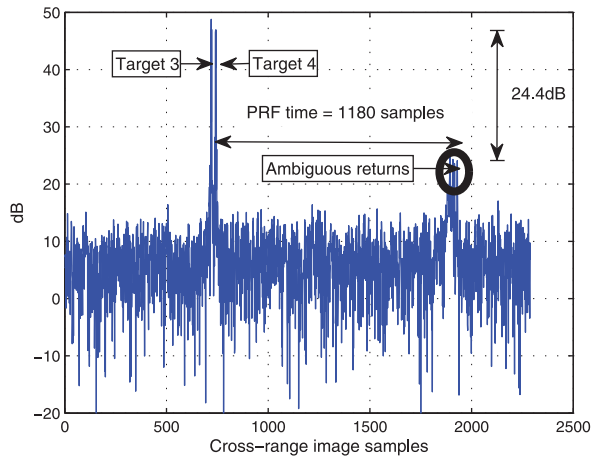

Fig. 12. Log slant range cut of reconstructed image across targets 3 and 4 using steering vector beamformer.

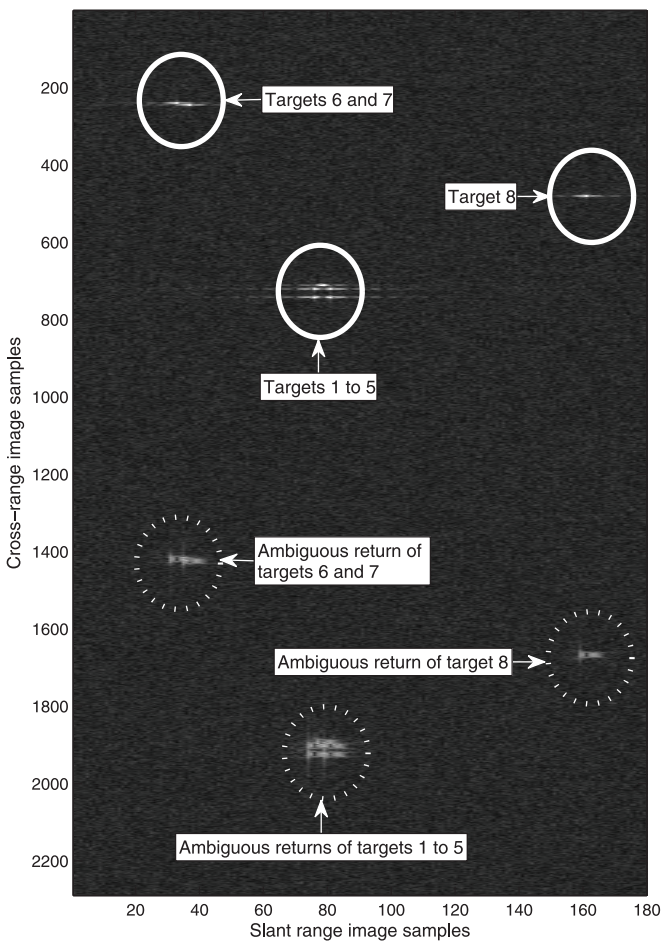

Fig. 11. Focused image after reconstruction using the steering vector beamformer.

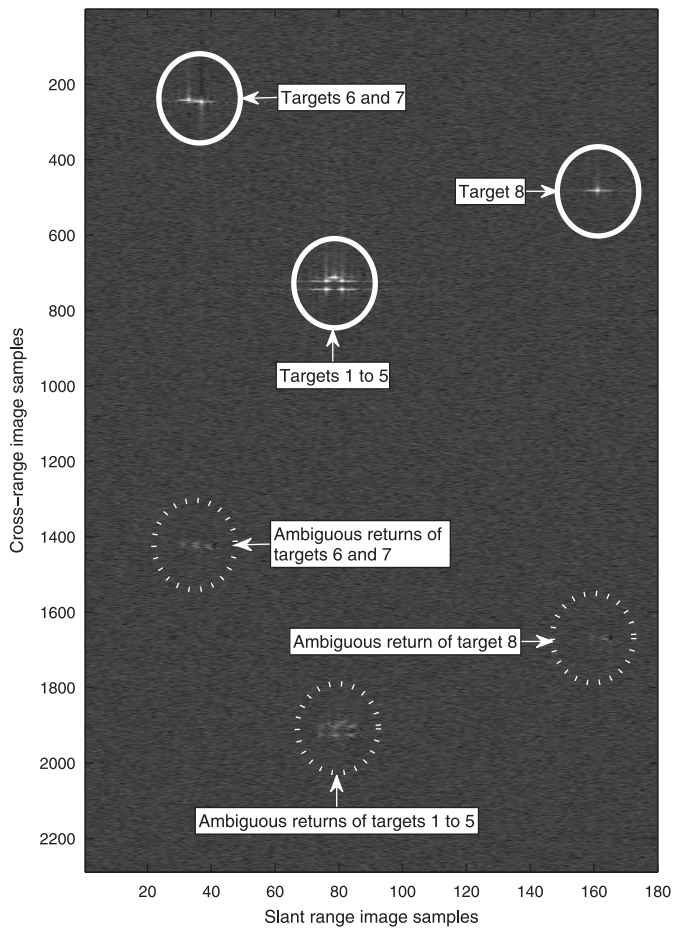

Fig. 13. Focused image after reconstruction using proposed beamformer.

is performed. From the undersampled data, the 3 dB width is 1.30 m. However when the steering vector beamformer is applied, this is improved to 0.32 m. When the proposed wide null beamformer is applied slight widening occurs resulting in a 3 dB width of 0.35 m compared to the steering vector beamformer.

B. Case 2: $M_d > 1$ With Sea Clutter

In this case an imaging environment with added sea clutter and a low SNR of -30 dB, is simulated with $M_d = 8$ targets, whose parameters are given in Table III and are shown in Fig. 8.

Fig. 9 shows the focused image of undersampled raw data and the ambiguous returns of the eight targets are clearly visible. With reference to Fig. 10, a slant range cut across targets 3 and 4 shows that the peak-to-ambiguity ratio is about 14.1 dB.

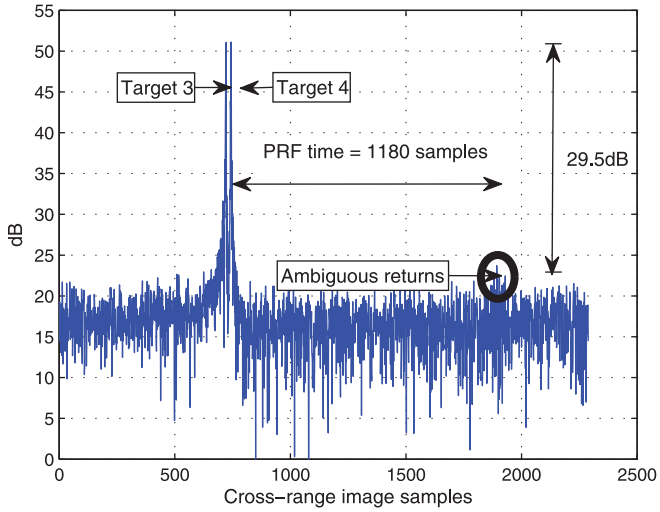

Fig. 14. Log slant range cut of reconstructed image across targets 3 and 4 using proposed beamformer.

By now performing reconstruction using the steering vector beamformer to give Fig. 11, it can be seen that the surrounding background of the targets is darker than in Fig. 9. Note that all images have been normalized and this darker background suggests a higher SNR. This can be seen in Fig. 12, showing a slant range cut across targets 3 and 4, where the noise level is about 10 dB, compared to around 25 dB in Fig. 10. Also from Fig. 12, it can be seen that there is an over 10 dB improvement in the peak-to-ambiguity ratio compared to when no reconstruction is applied, as shown in Fig. 10.

By now performing reconstruction using the proposed wide null beamformer, Fig. 13 is obtained. With reference to Fig. 14 it can also be seen that the peak-to-ambiguity ratio is improved from 24.4 dB when using the steering vector beamformer to 29.5 dB when using the proposed beamformer.

VI. Conclusion

In this paper, a novel superresolution beamformer capable of forming wide nulls using subspace based approaches for SIMO SAR systems forming a linear array along the cross-range direction has been proposed for the suppression of cross-range ambiguities in undersampled SAR data and reconstruction to form a single unambiguous set of SAR data. The use of the superresolution beamformer allows the wide swath, high resolution contradiction of SISO SAR to be overcome, allowing greater flexibility in meeting specific application requirements without being constrained by the swath width and cross-range resolution.

A SIMO SAR system has been designed and computer simulations for evaluation of the proposed beamformer has been shown to effectively allow the reconstruction of the $K > 1$ sets of undersampled SAR data. Compared to the steering vector beamformer, the proposed wide null beamformer only requires a single $(K \times 1)$ weight vector to suppress one block of ambiguous Doppler frequencies, as opposed to a $(K \times 1)$ weight vector for each ambiguous Doppler frequency. Also the proposed beamformer has been shown to give a better peak-to-ambiguity ratio.

Appendix A
The Steering Vector Beamformer

The technique detailed in [7] allows the reconstruction of the complete Doppler bandwidth from aliased subsampled signals received by a SIMO SAR system. As mentioned in [3], in the case of K collocated beamformers, this technique is equivalent to null-steering using the steering vector beamformer, where a manifold vector for all Doppler frequencies in the range $f_{d,k}$, described in (26) for $k = 1, 2, \ldots, K$, is formed, such that

$$\mathbb{S}(f_d) = \left[\underline{S}\left(f_{d,1}\right), \underline{S}\left(f_{d,2}\right), \ldots, \underline{S}\left(f_{d,K}\right)\right] \tag{43}$$

where the k^{th} column of $\mathbb{S}(f_d)$, $\underline{S}\left(f_{d,k}\right)$, is the manifold vector corresponding to the K beamformers for the k^{th} frequency range. The following weight matrix

$$\mathbb{W}(f_d) = \mathbb{S}^{-1}(f_d) \tag{44a}$$

$$= \left[\underline{w}_1(f_d), \underline{w}_2(f_d), \ldots, \underline{w}_K(f_d)\right]^T \tag{44b}$$

can then be formed such that the vector $\underline{w}_k$ is a $(K \times 1)$ weight vector which recovers the Doppler frequencies within the Doppler frequency range $f_{d,k}$ while suppressing the frequencies within the other $K - 1$ frequency ranges.

For the suppression of the ambiguous Doppler frequencies to form K sets of unambiguous data for each Doppler frequency range and combination to form a single set of data for each Doppler frequency range, the k^{th} row of $\mathbb{W}$ is applied to the received signals at the k^{th} receive beamformer in the Doppler domain[4]. The full Doppler spectrum can then be obtained by concatenating each Doppler frequency range, which results in unambiguous data in the cross-range direction.

By representing the weights for all f_d, the matrix $\mathbb{W}_k$ is defined as the weights applied to recover the k^{th} subband for all f_d within the subband

$$\mathbb{W}_k = \begin{bmatrix} \underline{w}_k\left(f_{d,1}\right), & \underline{0}_{K\times 1}, & \cdots & \underline{0}_{K\times 1} \\ \underline{0}_{K\times 1}, & \underline{w}_k\left(f_{d,2}\right), & \cdots & \underline{0}_{K\times 1} \\ \vdots & \vdots & \ddots & \vdots \\ \underline{0}_{K\times 1}, & \underline{0}_{K\times 1}, & \cdots & \underline{w}_k\left(f_{d,N_p}\right) \end{bmatrix} \tag{45}$$

for $k = 1, 2, \ldots, K$, and the reconstructed data can be given as

$$\mathbb{Y}_{recon}(f_d) = \left[\mathbb{W}_1^T \cdot \overline{\mathbb{X}}_c[f_d], \mathbb{W}_2^T \cdot \overline{\mathbb{X}}_c[f_d], \ldots, \mathbb{W}_K^T \cdot \overline{\mathbb{X}}_c[f_d]\right]^T \tag{46}$$

with

$$\overline{\mathbb{X}}_c[f_d] = \begin{bmatrix} \overline{\mathbb{X}}[f_{d,1}] \\ \overline{\mathbb{X}}[f_{d,2}] \\ \vdots \\ \overline{\mathbb{X}}\left[f_{d,N_p}\right] \end{bmatrix} \tag{47}$$

Appendix B
The Effect of K on the Selection of γ and τ_I

From (32), the values that γ, and consequently τ_I, can take is limited by the number of receive beamformers in the SIMO

[4]A Fourier transform on the received signals along the cross-range direction transforms the signals into the Doppler domain.

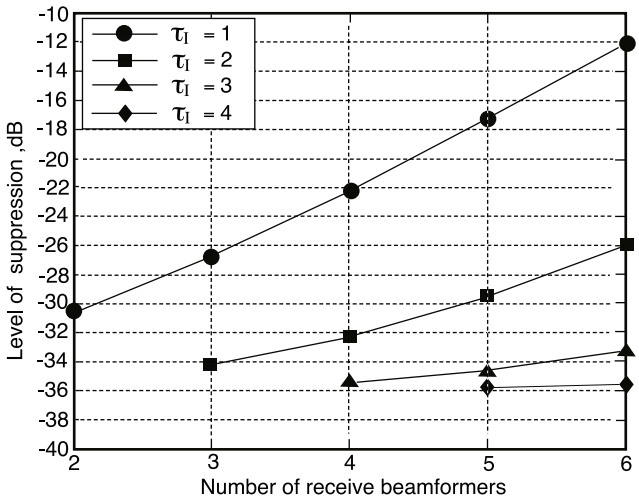

Fig. 15. Effect of the number of receive beamformers and value of τ_I on the level of suppression in dB.

SAR system. For suppression of a given ambiguous Doppler frequency range, $f_{d,I}$, using a linear array of $K > 1$ receive beamformers, it can be seen from Fig. 15 that with an increasing number of receive beamformers, the level of suppression of the ambiguous Doppler frequency range can be increased. Also the value of τ_I giving the greatest level of suppression increases with increasing K and care must be taken in the selection of τ_I to ensure that the benefits of an increased number of receive beamformers is used for increased ambiguous Doppler frequency suppression.

By relating back to Section V, in particular Fig. 13, the level of achieved suppression in the simulation is -29.5 dB, which is comparable to the calculated level of suppression in Fig. 15 for $K = 2$, which is -30.5515 dB.

REFERENCES

[1] A. Currie and M. A. Brown, "Wide-swath SAR," in *IEE Proc. Radar Signal Process.*, Apr. 1992, vol. 139, no. 2, pp. 122–135.
[2] A. Freeman, "On ambiguities in SAR design," in *Proc. EUSAR*, 2006.
[3] N. Gebert, G. Krieger, and A. Moreira, "Digital beamforming on receive: Techniques and optimization strategies for high-resolution wide-swath SAR imaging," *IEEE Trans. Aerosp. Electron. Syst.*, vol. 45, no. 2, pp. 564–592, Apr. 2009.
[4] M. Younis, C. Fisher, and W. Wiesbeck, "Digital beamforming in SAR systems," *IEEE Trans. Geosci. Remote Sens.*, vol. 41, no. 7, pp. 1735–1739, Jul. 2003.
[5] G. Krieger, "MIMO-SAR: Opportunities and pitfalls," *IEEE Trans. Geosci. Remote Sens.*, vol. 52, no. 5, pp. 2628–2645, May 2014.
[6] M. Younis, F. Bordini, N. Gebert, and G. Krieger, "Smart multi-aperture radar techniques for spaceborne remote sensing," in *Proc. IEEE Int. Geosci. Remote Sens. Symp.*, Jul, 2008, vol. 3, pp. 278–281.
[7] G. Krieger, N. Gebert, and A. Moreira, "Unambiguous SAR signal reconstruction from nonuniform displaced phase center sampling," *IEEE Geosci. Remote Sens. Lett.*, vol. 1, no. 4, pp. 260–264, Oct. 2004.
[8] P. Karaminas and A. Manikas, "Super-resolution broad null beamforming for cochannel interference cancellation in mobile radio networks," *IEEE Trans. Veh. Technol.*, vol. 49, no. 3, pp. 689–697, May 2000.
[9] A. Manikas, *Differential Geometry in Array Processing*. London, U.K.: Imperial College Press, 2004.
[10] A. Haimovich and M. Berin, "Eigenanalysis-based space-time adaptive radar: Performance analysis," *IEEE Trans. Aerosp. Electron. Syst.*, vol. 33, no. 4, pp. 1170–1179, Oct. 1997.
[11] J. Guerci and J. Bergin, "Principal components, covariance matrix tapers, and the subspace leakage problem," *IEEE Trans. Aerosp. Electron. Syst.*, vol. 38, no. 1, pp. 152–162, Jan. 2002.
[12] H. Wang and L. Cai, "On adaptive spatial-temporal processing for airborne surveillance radar systems," *IEEE Trans. Aerosp. Electron. Syst.*, vol. 30, no. 3, pp. 660–670, Jul. 1994.
[13] J. Guerci, J. Goldstein, and I. Reed, "Optimal and adaptive reduced-rank STAP," *IEEE Trans. Aerosp. Electron. Syst.*, vol. 36, no. 2, pp. 647–663, Apr. 2000.
[14] R. Fa, R. de Lamare, and L. Wang, "Reduced-rank STAP schemes for airborne radar based on switched joint interpolation, decimation and filtering algorithm," *IEEE Trans. Signal Process.*, vol. 58, no. 8, pp. 4182–4194, Aug. 2010.
[15] R. Fa and R. de Lamare, "Reduced-rank STAP algorithms using joint iterative optimization of filters," *IEEE Trans. Aerosp. Electron. Syst.*, vol. 47, no. 3, pp. 1668–1684, Jul. 2011.
[16] J. Ender, "Space-time adaptive processing for synthetic aperture radar," *IEE Colloquium Space-Time Adaptive Process.*, pp. 6/1–6/18, Apr. 1998.
[17] S. DeGraaf, "SAR imaging via modern 2-D spectral estimation methods," *IEEE Trans. Image Process.*, vol. 7, no. 5, pp. 729–761, May 1998.
[18] L. Rosenberg and D. Gray, "Anti-jamming techniques for multichannel SAR imaging," in *IEE Proc. on Radar, Sonar, Navig.*, Jun. 2006, vol. 153, no. 3, pp. 234–242.
[19] I. G. Cumming and F. H. Wong, *Digital Processing of Synthetic Aperture Radar Data*. Norwell, MA, USA: Artech House, 2005.
[20] N. Gebert, F. de Almeida, and G. Krieger, "Airborne demonstration of multichannel SAR imaging," *IEEE Geosci. Remote Sens. Lett.*, vol. 8, no. 5, pp. 963–967, Sep. 2011.
[21] J.-H. Kim, M. Younis, P. Prats-Iraola, M. Gabele, and G. Krieger, "First spaceborne demonstration of digital beamforming for azimuth ambiguity suppression," *IEEE Trans. Geosci. Remote Sens.*, vol. 51, no. 1, pp. 579–590, Jan. 2013.

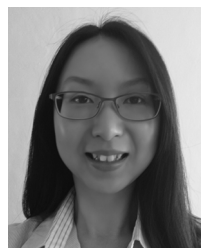

Karen Mak received the Master of Engineering (M.Eng.) degree in electrical and electronic engineering from Imperial College London, U.K., in 2006. In 2010 she started her Ph.D. work in the area of arrayed synthetic aperture radar under the supervision of Professor A. Manikas and her research was fully funded by an Engineering and Physical Science Research Council (EPSRC) Doctoral Training Award. In 2015, she received her Ph.D. degree from Imperial College London.

Her research interests lie in the areas of wireless communications, array processing, SIMO and MIMO synthetic aperture radar, beamforming, and superresolution direction finding algorithms.

Athanassios Manikas received the Ph.D. degree from the University of London and the D.I.C. diploma from Imperial College London, U.K., in 1988. Professor Manikas is a Fellow of the Institution of Engineering and Technology (IET) and Fellow of the Institute of Mathematics and its Applications (IMA). He holds the Chair in Communications and Array Processing in the Department of Electrical and Electronic Engineering, Imperial College London and was the Technical Lead of the MOD-UK University Defence Research Centre in Signal Processing (DSTL/EPSRC) from its establishment until 2013.

He has published an extensive set of journal and conference papers in the area of digital wireless communications and array signal processing and is the Author of a book (monograph) entitled "Differential Geometry in Array Processing."

He is on the editorial board of IET Signal Processing and is also the Editor of the ICPress research book-series on Communications and Signal Processing.

He has held a number of research consultancies for the EU, industry and government organizations. He has had various technical chairs at international conferences including the IEEE International Conference on Communications in 2015 (IEEE ICC 2015 London). He has served as an Expert Witness in the High Court of Justice (UK) and was a member of the Royal Society's International Fellowship Committee (2008–2011). He is currently the vice-Chair of the IEEE Communications Technical Committee on Transmission, Access and Optical Systems (TAOS).

Professor Manikas is leading a strong group of researchers at Imperial College and has supervised successfully more than 45 Ph.D.s and more than 200 Masters project-students.